ACS OMEGA

Article

Cite This: ACS Omega 2018, 3, 1187−1196

Scale-Up Fabrication of Biodegradable Poly(butylene adipate-*co*-terephthalate)/Organophilic−Clay Nanocomposite Films for Potential Packaging Applications

Jiazhuo Xie,[†,§] Zhou Wang,[‡] Qinghua Zhao,[†,∥] Yuechao Yang,[§] Jing Xu,[*,†] Geoffrey I. N. Waterhouse,[†,⊥] Kun Zhang,[†] Shan Li,[§] Peng Jin,[§] and Geyang Jin[§]

[†]College of Chemistry and Material Science, Shandong Agricultural University, 61 Daizong Street, Tai'an 271000, Shandong, China

[‡]State Key Laboratory of Nutrition Resources Integrated Utilization, Kingenta Ecological Engineering Co., Ltd, 19 Xingdaxi Street, Linshu 276700, Shandong, China

[§]National Engineering Laboratory for Efficient Utilization of Soil and Fertilizer Resources, National Engineering & Technology Research Center for Slow and Controlled Release Fertilizers, College of Resources and Environment, Shandong Agricultural University, 61 Daizong Street, Tai'an 271000, Shandong, China

[∥]Department of Basic Courses, Shandong Medicine Technician College, 999 Fengtian Road, Tai'an 271000, Shandong, China

[⊥]School of Chemical Sciences, The University of Auckland, Private Bag 92019, Auckland 1142, New Zealand

Supporting Information

ABSTRACT: The development of biodegradable packing materials is a global priority due to the huge volumes of plastic refuse entering landfills and the environment. In this study, a series of biodegradable nanocomposite films based on poly(butylene adipate-*co*-terephthalate) (PBAT) and reinforced with an organophilic layered double hydroxide (OLDH) were scale-up fabricated. The OLDH nanosheets with a basal spacing of 4.07 nm were presynthesized on a large-scale by solvent-free high-energy ball milling. All of the PBAT/OLDH nanocomposite films (0.5−4 wt % OLDH) showed a uniform dispersion of OLDH nanosheets in the PBAT matrix. A PBAT/OLDH film containing 1 wt % OLDH (denoted herein as OLDH-1) demonstrated outstanding thermal, optical, mechanical, and water vapor barrier properties compared with a pure PBAT film (OLDH-0), including a 37% reduction in haze and a 41.9% increase in nominal tensile strain at break dramatically. Furthermore, the food packaging measurement revealed that the OLDH-1 film showed a better packaging effect than the pure PBAT film and commercial polyethylene packing materials. The feasibility of scale-up manufacture and the excellent processability, manufacturing scalability, mechanical performance, optical transparency, water vapor barrier properties, and food packaging performance of the PBAT/OLDH nanocomposite films encourage their future application as biodegradable packaging films.

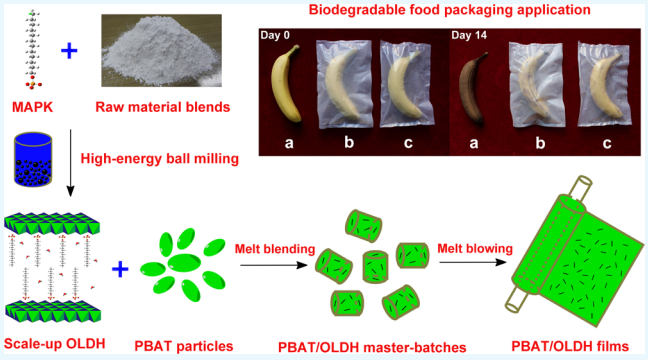

INTRODUCTION

Despite the worldwide application of the commercial petrochemical-based packaging materials nowadays, enormous research effort has been devoted to solve the problem of non-biodegradable food packaging materials, motivated in large part by increasing the awareness of environmental problems caused by plastics entering landfills and the wider environment.[1−5] Furthermore, the excessively strong barrier ability of these packaging materials for water can produce local environment with high humidity when used to pack fruits, giving rise to the possible rapid reproduction of microorganism and therefore accelerating the aging and spoilage process. Based on these disadvantages, to develop ecofriendly biodegradable polymeric packaging materials with appropriate water barrier abilities, many biodegradable polymers, such as polylactide, poly(propylene carbonate), and poly(butylene adipate-*co*-terephthalate) (PBAT), have been extensively investigated in the context.[6−10]

Poly(butylene adipate-*co*-terephthalate) is a aliphatic−aromatic copolyester thermoplastic that can be blended with other polymeric materials (e.g., polylactic acid) to produce a broad range of plastic film materials for different applications.[11−14] Although it shows excellent processability, film-forming property, and biodegradability, the optical, mechanical, and water vapor barrier properties of PBAT still need to be improved to match those of the conventional non-biodegrad-

Received: December 25, 2017
Accepted: January 9, 2018
Published: January 30, 2018

DOI: 10.1021/acsomega.7b02062
ACS Omega 2018, 3, 1187−1196

able petrochemical-based counterparts, such as linear low density polyethylene.[15,16] One of the most effective approaches for enhancing the properties of polymers is to introduce nanofillers at low loadings (typically <5 wt %).[17−19] Recently, montmorillonite or layered silicates have been added to PBAT to enhance the thermal, mechanical, rheological, and barrier properties of the polymer.[20,21] However, the ammonium ions in the interlayer space of montmorillonite were easily degraded or lost during the PBAT composite-manufacturing process, thereby compromising the integrity and properties of the composite.[22] Therefore, the correct choice of filler is important to achieving improved functionality.

Layered double hydroxides (LDHs) are layered claylike materials composed of sheets of positively charged edge-sharing MO_6 octahedra with charge-balancing anions and water occupying the interlayer space between the sheets.[23] LDHs have the general formula $[M^{2+}_{1-x}M^{3+}_{x}(OH)_2]^{q+}(A^{n-})_{q/n}\cdot yH_2O$ (where M^{2+} = Mg^{2+}, Co^{2+}, Ni^{2+}, Cu^{2+} or Zn^{2+}; M^{3+} = Al^{3+} or Cr^{3+}; and A^{n-} are the charge-balancing anions).[24,25] Due to their compositional flexibility, LDH find widespread application in sorption and catalysis.[26] However, the abundance of hydroxyl groups on the surface of the LDH sheets makes them hydrophilic.[27] To obtain better compatibility with polymer matrix,[28] LDH was often modified by replacing its interlayer anions (typically NO_3^- or CO_3^{2-}) with large organic anions to yield organophilic layered double hydroxides (OLDHs) with a much lower hydrophilicity. Recently, biodegradable OLDH-containing polymeric composites have been studied, with good enhancements reported in the optical, mechanical, and barrier properties resulting from the OLDH addition.[29−31] However, the dominating preparation of OLDH was to first synthesize the LDH precursor in aqueous solutions and then obtain the OLDH by organic modification. There are some shortcomings: (1) low yield, (2) complicated process, (3) solvents use, (4) overlong reaction time, and (5) high reaction temperature. This limited the application of this anion-exchange route. Therefore, it is a key point to scale-up the fabrication of OLDH. High-energy ball milling method, which is amenable for the large-scale synthesis of LDH materials in "one pot", has recently attracted much interest.[32,33] The advantages were obvious, such as simple, unheated, solvent-free preparation process and a large-scale yield. To the best of our knowledge, the direct large-scale synthesis of OLDH by high-energy ball milling has a scarce report, although obviously has great potential for practical applications. Based on the advantages, the large-scale yield of OLDH made it possible to develop the PBAT/OLDH films as a commercial packaging application.

The overarching objective of this work was the scale-up the fabrication of biodegradable PBAT/OLDH nanocomposite films by the commonly used melt blending and blowing process.[34] The OLDH-containing organic aliphatic long-chain anion was successfully synthesized on a large scale by high-energy ball milling method. The Fourier transform infrared (FT-IR) spectrum, X-ray diffraction (XRD), and transmission electron microscopy (TEM) were employed to verify the formation of nanosized OLDH. Particular emphasis is placed on the effect of the OLDH loading (0, 0.5, 1, 2, and 4 wt %, which is denoted as OLDH-0, OLDH-0.5, OLDH-1, OLDH-2, and OLDH-4) on the structure and properties (e.g., processability, thermal, optical, mechanical, water vapor barrier properties, and food packaging performance) of the PBAT/OLDH nanocomposite films as a benchmark of their potential for commercial packaging applications.

RESULTS AND DISCUSSION

Fabrication and Processability of the PBAT/OLDH Nanocomposite Films. Intermolecular interactions between the PBAT macromolecular chains (primarily van der Waals interactions between aromatic−aromatic and hydrogen bonding of neighboring PBAT molecules) enhance fluid friction and cause PBAT polymer melts to be viscous,[35] resulting in melt blown PBAT films that are sticky and difficult to separate. In this work, the incorporation of an OLDH into the PBAT matrix is found to be highly effective in improving the processability of the polymer. The PBAT/OLDH composites could be melted and blown into films without any difficulty, whereas the obtained films display none of the stickiness typical of pure PBAT films. The improved processability of PBAT/OLDH is attributed to the lubricating effect of OLDH to reduce chain entanglement and friction along the molecular chains. As expected, thermal degradation of organic anion intercalator in OLDH ($C_{12}H_{25}PO_4^{2-}$, thermal decomposition temperature: 236 °C) does not occur during the melt blending and blowing steps used for composite film fabrication.

Structural and Morphological Characterization of the OLDH and the PBAT/OLDH Films. The FT-IR, XRD, TEM, and scanning electron microscopy (SEM) are employed to characterize the structural and morphological characterization of the OLDH and the PBAT/OLDH films. The FT-IR spectra for the OLDH powder and PBAT/OLDH films (OLDH-0, OLDH-4) are shown in Figure 1. For the OLDH spectra in

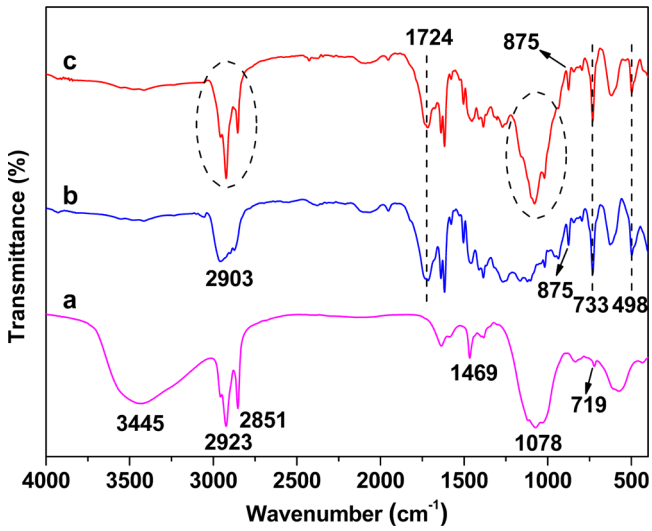

Figure 1. FT-IR spectra of (a) OLDH powder and PBAT/OLDH films: (b) OLDH-0 and (c) OLDH-4.

Figure 1a, the peaks are associated with C−H stretching (2923 and 2585 cm^{-1}), CH_2 scissoring (1469 cm^{-1}), P═O and/or P−O stretching (1078 cm^{-1}), and $(CH_2)_n$ rocking vibrations (719 cm^{-1})[36,37] with $C_{12}H_{25}PO_4^{2-}$ anions in the interlayer region of OLDH. The strong and broad absorption peaks at 3445 cm^{-1} can be attributed to the O−H stretching modes of the hydroxyl groups on the OLDH sheets and also the water molecules in the interlayer region.

The FT-IR spectrum of OLDH-0 in Figure 1b is similar to that previously reported for PBAT,[38] showing characteristic peaks at 2901, 1724, 875, 733, and 498 cm^{-1}, which could readily be assigned to the aliphatic and aromatic C−H stretching, C═O stretching, C−O stretching, C═C stretching,

DOI: 10.1021/acsomega.7b02062
ACS Omega 2018, 3, 1187−1196

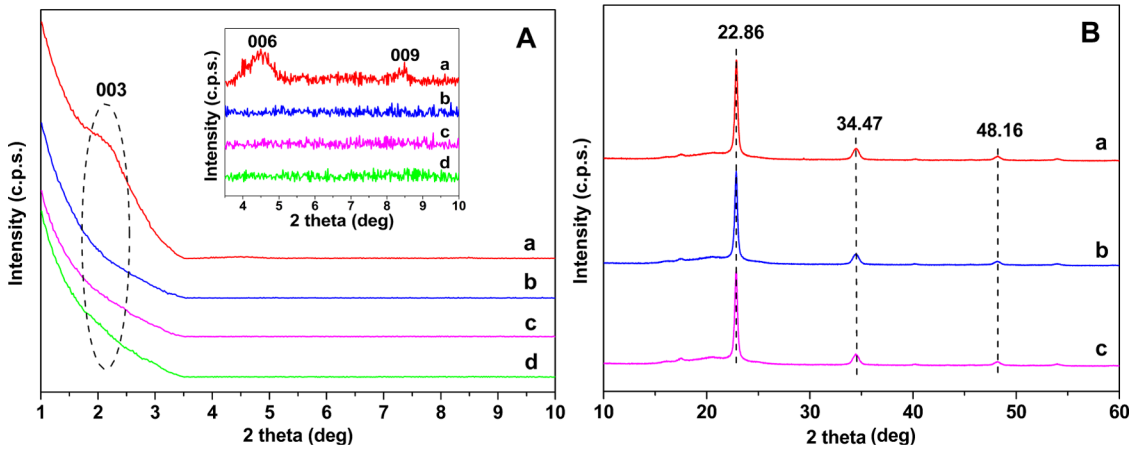

Figure 2. (A) X-ray diffraction patterns for (a) OLDH powder and PBAT/OLDH films: (b) OLDH-0, (c) OLDH-1, and (d) OLDH-4 in the 2θ range of 1−10°. (B) XRD patterns of PBAT/OLDH films: (a) OLDH-0, (b) OLDH-1, and (c) OLDH-4 in the 2θ range of 10−60°.

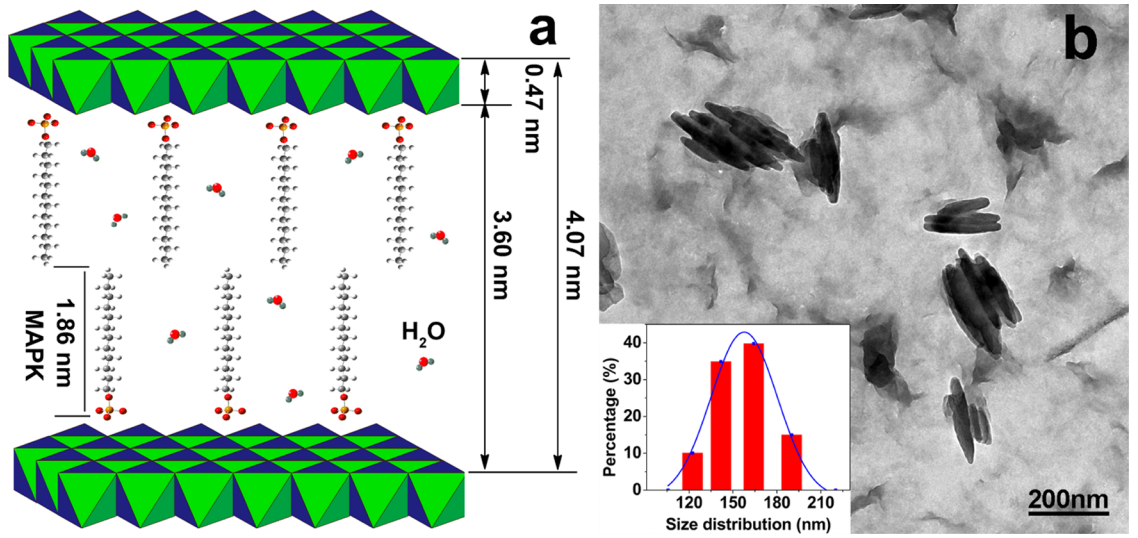

Figure 3. (a) Schematic showing the arrangement of MAPK anions in the OLDH interlayer region. (b) TEM images and size distribution of the OLDH.

and CH_2 rocking modes of the polymer. The FT-IR spectrum of OLDH-4 in Figure 1c contains contributions from both OLDH and PBAT matrices. In particular, the observation of intense peaks at 2923, 2851, and 1078 cm^{-1} associated with $C_{12}H_{25}PO_4^{2-}$ anions in OLDH in the FT-IR spectrum of the composite provides a strong evidence for the successful incorporation of OLDH nanosheets into the PBAT matrix.

To further confirm the structural characterization, XRD was performed to detect the structure of the OLDH powder and the PBAT/OLDH films (OLDH-0, OLDH-1, and OLDH-4) in Figure 2. The XRD pattern for the OLDH powder in Figure 2A,a contains peaks at 2θ = 2.17, 4.70, and 8.45°, which can readily be assigned to the (003), (006), and (009) reflections of a layered double hydroxide material with a well-developed layer structure.[39] The basal spacing d(003) was 4.07 nm, similar to that reported for the OLDH obtained from LDH by the anion-exchange method in our previous work.[40] Considering the alkyl chain length of mitogen activated protein kinase (MAPK) (1.86 nm) and the thickness of metal hydroxide layer (0.47 nm) in the LDH sheets, it can be concluded the MAPK anion chains are arranged in a bilayer (two molecules thick) between the metal hydroxide sheets, as shown in Figure 3a.

The XRD patterns for a selection of PBAT/OLDH composite films (OLDH-0, OLDH-1, and OLDH-4 containing 0, 1, and 4 wt % OLDH, respectively), are shown in Figure 2A,b−d. The XRD data for all three films are identical. The characteristic (003), (006), and (009) reflections of OLDH cannot be discerned in the XRD patterns of OLDH-1 and OLDH-4, which can be attributed to the very low OLDH loadings in the films or possibly partial delamination of the metal hydroxide sheets of OLDH in the PBAT matrix. Crystalline reflections associated with the PBAT matrix are observed at higher 2θ angles of 22.86, 34.47, and 48.16° in Figure 2B,a−c. The XRD data for OLDH-0, OLDH-1, and OLDH-4 in this region are identical, confirming that the OLDH addition at loadings up to 4 wt % have no adverse effect on the crystalline structure or crystallinity of PBAT films.

The TEM and SEM analyses are performed to confirm the morphological characterization of the OLDH and the PBAT/OLDH composite films. The TEM image and size distribution of OLDH reveals that the OLDH is in nanoscale, with size distribution 100−200 nm in Figure 3b. The SEM micrographs of the fracture surface of OLDH-0, OLDH-1, and OLDH-4 are shown in Figure 4. The fracture surface of OLDH-0 is smooth,

DOI: 10.1021/acsomega.7b02062
ACS Omega 2018, 3, 1187−1196

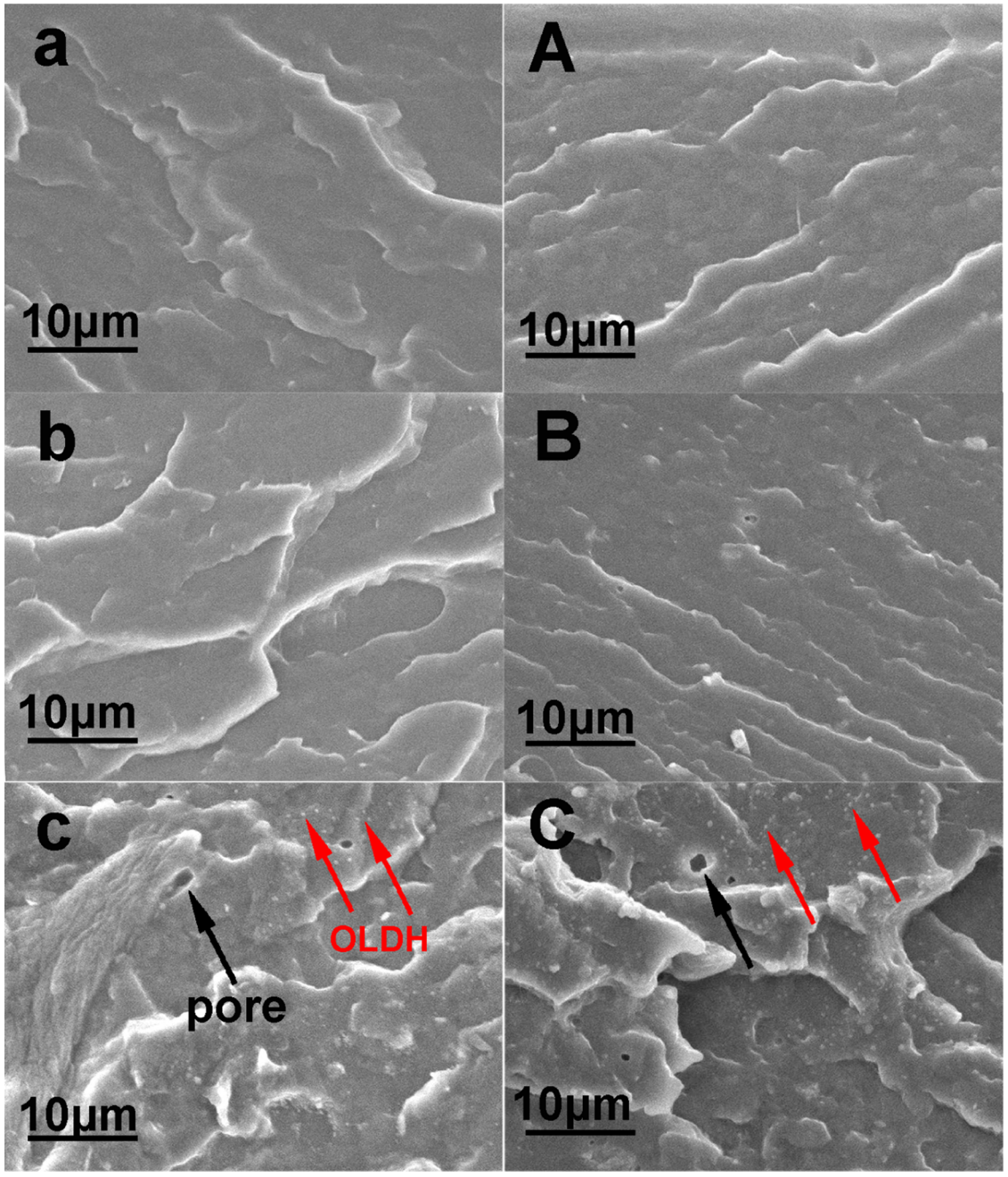

Figure 4. SEM images of the fracture surfaces of PBAT/OLDH composite films: (a, A) OLDH-0, (b, B) OLDH-1, and (c, C) OLDH-4, where (a)−(c) are the images in transverse direction and (A)−(C) in the machine direction, respectively.

showing no pores (Figure 4a,A). The SEM images for OLDH-1 are very similar to those collected for OLDH-0 (Figure 4b,B). OLDH-4 shows a very uniform dispersion of small OLDH nanoparticles (signed by red arrows) in the PBAT matrix (Figure 4c,C), an evidence for good compatibility between the two composite components. It should be noted that OLDH-4 also contains a number of small pores, which likely result from the release of water from the OLDH interlayer region during the composite-manufacturing process.[41] This would explain why the amount of pores in the films increased with the OLDH content.

Thermal Analysis of PBAT/OLDH Films. To study the thermal stability of a selection of PBAT/OLDH films (OLDH-0, OLDH-1, and OLDH-4), differential scanning calorimetry (DSC) is employed to analyze the crystallization and melting behavior. The cooling and heating curves are presented in Figure 5A,B, respectively. OLDH-0 shows a crystallization temperature (T_c) of 82.28 °C on cooling from the melt (Figure 5A). The crystallization temperature for OLDH-1 is higher (84.02 °C) than that of OLDH-0, which is explained by the heterogeneous nucleation caused by the presence of the OLDH platelets, which promote polymer crystallite growth, in the PBAT matrix.[42] However, the higher loadings of OLDH in the PBAT/OLDH composites lowers the T_c (e.g., OLDH-4, T_c 81.21 °C), suggesting that excessive amounts of OLDH can interfere with the crystallization of PBAT. This result is not surprising because polymer crystallization requires parallel alignment of the polymer chains and the formation of lamellae,

DOI: 10.1021/acsomega.7b02062
ACS Omega 2018, 3, 1187−1196

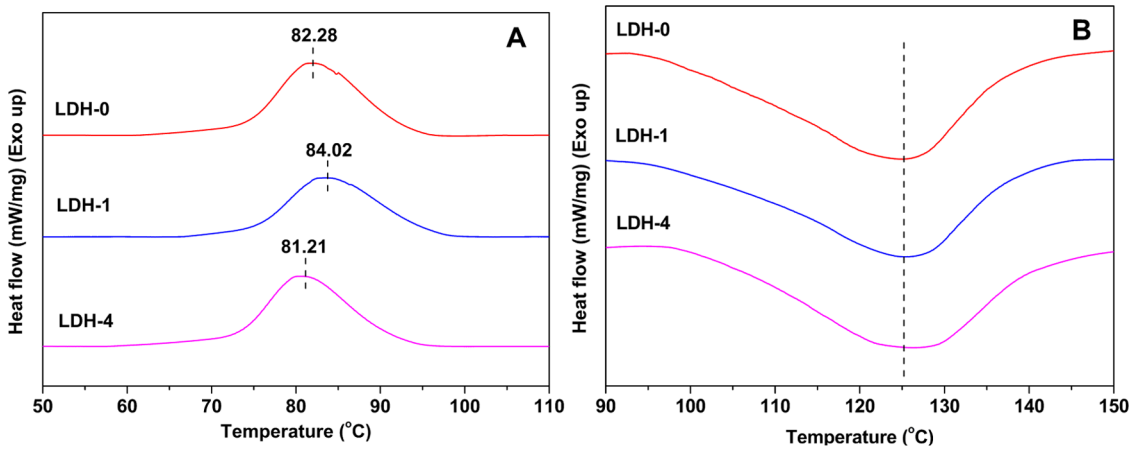

Figure 5. DSC cooling traces (A) and heating traces (B) for PBAT/OLDH nanocomposite films: OLDH-0, OLDH-1, and OLDH-4.

processes that will be kinetically hindered by excessive amounts of impurities (i.e., too many OLDH nanosheets). In contrast, the melting temperatures (T_m) of the PBAT/OLDH films (OLDH-1 and OLDH-4) are almost identical to that of pure PBAT (i.e., OLDH-0), as shown in Figure 5B. However, the melting curves become progressively broader with increasing OLDH content, suggesting some minor influence of the OLDH nanosheets on the melting properties of the composite films.

Optical Properties of the PBAT/OLDH Films. Visible light transmittance and haze are key properties for packaging films, with a high transmittance and low haze being desirable. A detailed investigation of the PBAT/OLDH films is thus undertaken. Figure 6 shows that the visible light transmittance

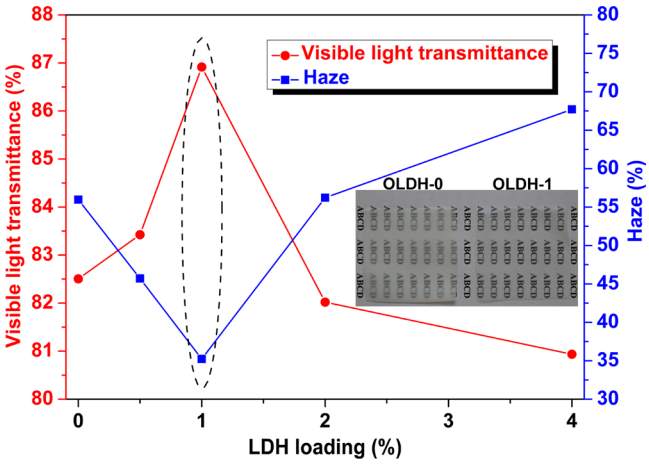

Figure 6. Visible light transmittance and haze curves of PBAT/OLDH films: OLDH-0, OLDH-0.5, OLDH-1, OLDH-2, and OLDH-4.

of the PBAT/OLDH films improve with the OLDH content up to 1 wt %, and then decreases sharply at higher OLDH loadings. The haze decreases with OLDH addition up to 1 wt % and then increases again at higher loadings. The OLDH-1 film thus display the best optical properties among the films tested, showing a 5% higher optical transmittance and a 37% lower haze than the pristine PBAT film. This can be attributed to an increase in the nucleation sites in the polymer-crystallizing process and the amorphous form of PBAT matrix induced by the heterogeneous nucleation effect of the OLDH nanosheets, which is also supported by the DSC data in Figure 5A. The progressive deterioration of the optical properties of the films at higher OLDH loadings (i.e., above 1 wt %) can be attributed to the scattering effects caused by the development of small pores (cf. Figure 4c,C). The superior optical property of the OLDH-1 film compared to the OLDH-0 (pristine PBAT film) is visibly evident from the digital photographs shown in Figure 6.

Mechanical Properties of PBAT/OLDH Films. The mechanical properties of the PBAT/OLDH films are evaluated in the transverse direction and machine direction, with results presented in Figure 7A,B, respectively. The data show that the

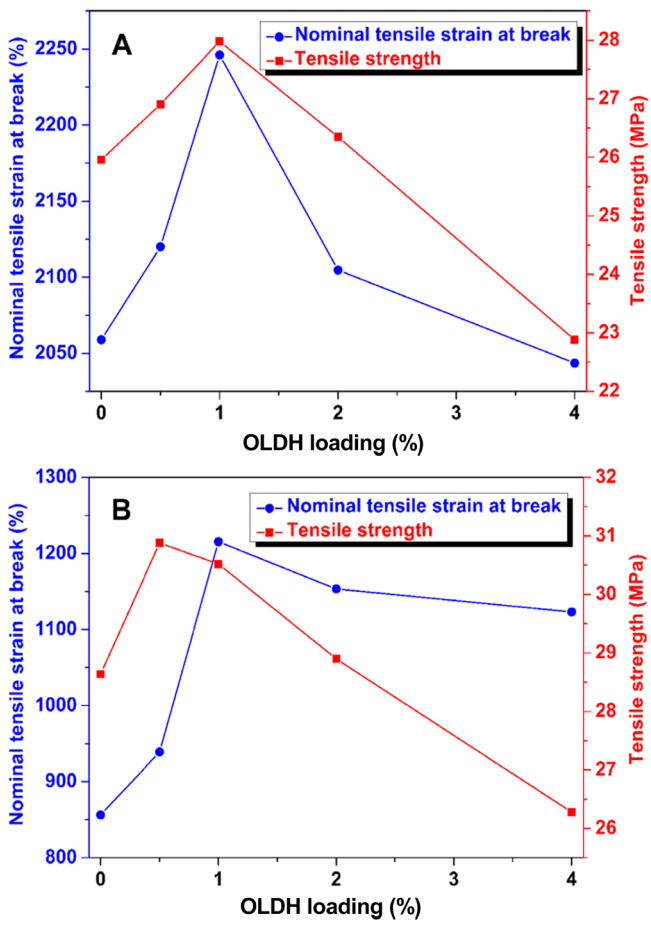

Figure 7. Tensile properties of PBAT/OLDH films: OLDH-0, OLDH-0.5, OLDH-1, OLDH-2, and OLDH-4 in (A) transverse direction and (B) machine direction.

DOI: 10.1021/acsomega.7b02062
ACS Omega 2018, 3, 1187−1196

nominal tensile strain at break and the tensile strength of the PBAT/OLDH films in both the transverse and machine directions increase with OLDH loading up to an optimum OLDH loading of ∼1 wt %. In particular, OLDH-1 shows a 41.9% improvement in the nominal tensile strain at break in the machine direction compared with OLDH-0 (PBAT with no OLDH added). It can be concluded that the OLDH addition at low loadings leads to significant enhancement in the tensile properties of the PBAT/OLDH films, especially the nominal tensile strain at break in the machine direction. At high OLDH loadings (>1 wt %), the intermolecular interactions between PBAT molecular chains are interrupted by the abundance of OLDH nanosheets and pores in the polymer matrix, weakening the mechanical strength of the films.

The enhancement of the tensile properties of PBAT with OLDH addition at low loadings warrants further discussion. PBAT is a flexible polymer, whereas the OLDH particles are rigid fillers. Therefore, the increase in the tensile strength and the nominal tensile strain at break for OLDH-1 is likely related to the high aspect ratio of the OLDH nanosheets and their homogeneous dispersion within the PBAT matrix.[43,44] The enhancement in the mechanical properties in the machine direction in the nanocomposite hybrids likely results from a uniform alignment of the OLDH nanosheets in the plane of the PBAT films caused by the shear stress during the film manufacture, and also the excellent interfacial contact of the PBAT chains with the OLDH nanosheets.[45]

Water Vapor Barrier Properties of PBAT/OLDH Films. The water vapor transmission properties of the PBAT/OLDH films are investigated to evaluate the effect of the OLDH content on the water vapor barrier properties of the films. The water vapor transmission rate (WVTR) of each sample is calculated according to the following eq 1

$$\mathrm{WVTR}\ (\mathrm{g\ m^{-2}{\cdot}24\ h}) = (24{\cdot}\Delta m)/(A{\cdot}t) \quad (1)$$

where Δm (g) is the mass of water vapor passing through the sample film; A (m^2) is the area of each film; and t (h) is the measured time interval. As shown in Figure 8, the addition of OLDH decreases the WVTR of PBAT markedly. The WVTR decreases by 11.6 and 14.3% for OLDH-1 and OLDH-2, respectively, compared with OLDH-0. This can be explained by the presence of the OLDH nanoparticles in the film, creating a longer diffusion path for water molecules to pass through the film. It is probable that the OLDH nanosheets are delaminated to some extent in the films, giving an abundance of two-dimensional nanoplatelets with a uniform dispersion throughout the PBAT matrix, further extending the path taken by water molecules in traversing the PBAT/OLDH films.[46] This is depicted schematically in Figure 8. The improvement in the water vapor barrier properties of PBAT on OLDH addition at low loadings is of great importance in the food packaging field.

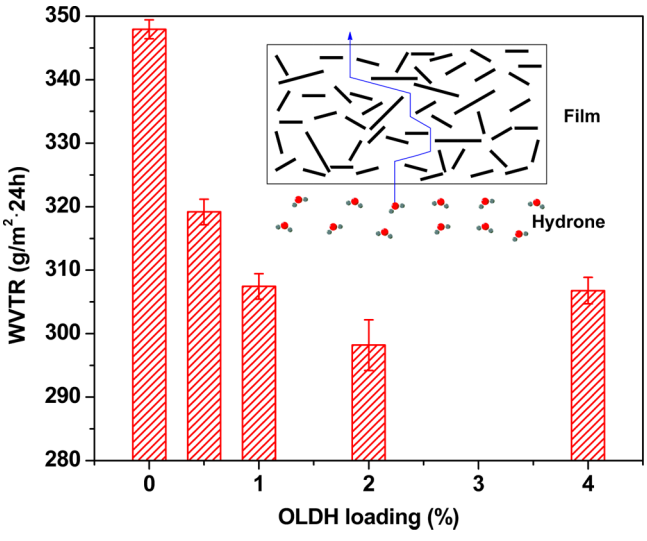

Figure 8. WVTR of different PBAT/OLDH films: OLDH-0, OLDH-0.5, OLDH-1, OLDH-2, and OLDH-4 and the water vapor barrier mechanism of PBAT/OLDH films containing OLDH nanosheets.

Food Packaging Experiment. Banana is a delicious and worldwide fruit containing abundant vitamin B and mineral substances. However, the easy aging and spoilage has made the storage of banana a hot topic. At present, the common strategy to store banana are packaging with petrochemical-based polymer films. The ideal packaging materials can prevent the spoilage and keep the freshness of fruit. However, the local environment with high humidity (Figure S1) produced by the excessively strong water barrier ability of the present commercial packaging materials will accelerate the aging and spoilage process of banana. Among the extensively recognized ecofriendly polymers, PBAT with appropriate water barrier ability compared with those of petrochemical-based polymer, make it possible as a better packaging material to store fruits. Therefore, we select PBAT as the test object to solve the easy spoilage of banana.

In our work, the food packaging experiment of the pure PBAT film and PBAT/OLDH films with enhanced water barrier ability are taken to evaluate the feasibility as a food packaging film.[47] Considering that the OLDH-1 film demonstrates outstanding thermal, optical, mechanical, and water vapor barrier properties compared with other PBAT/OLDH films (OLDH-0.5, OLDH-2, and OLDH-4) and pure PBAT film (OLDH-0), we chose the OLDH-1 film and pure PBAT film as experimental subject. The result is significantly obvious. As shown in Figure 9, the banana sample packaged with OLDH-1 film demonstrates the optimal color and luster than that packaged with pure PBAT film and exposed to air after 14 days. This reveals that the PBAT/OLDH nanocomposite film containing 1% OLDH shows a better packaging effect than other PBAT films, which is contributed by the better watertightness of the PBAT/OLDH nanocomposite film. Furthermore, the contrastive banana packaging experiment (Figure S2) reveals that the banana packed with PBAT/OLDH film had better color and luster than that packed with commercial polyethylene film after 14 days. Interestingly, the obvious accumulation of water released by banana itself and the white bacterial colony of banana packed by polyethylene film (Figure S2) after 56 days can further verify the excessively strong water barrier ability of the present commercial packaging materials, which can easily result in the spoilage of bananas. The results encourage the future food packaging application of biodegradable PBAT/OLDH film.

CONCLUSIONS

A series of biodegradable nanocomposite films based on poly(butylene adipate-*co*-terephthalate) (PBAT) and an organophilic layered double hydroxide (OLDH) were fabricated at industrial level using a melt blending and blowing method. High-energy ball milling was used to synthesize an OLDH, yielding a pure product in a high yield, with large alkyl

DOI: 10.1021/acsomega.7b02062
ACS Omega 2018, 3, 1187−1196

Figure 9. Photographs of banana samples with following treatment: (a) exposed to air, (b) packaged with pure PBAT film, and (c) packaged with OLDH-1 film.

Scheme 1. Schematic Illustration for the Manufacture of the Biodegradable PBAT/OLDH Nanocomposite Films

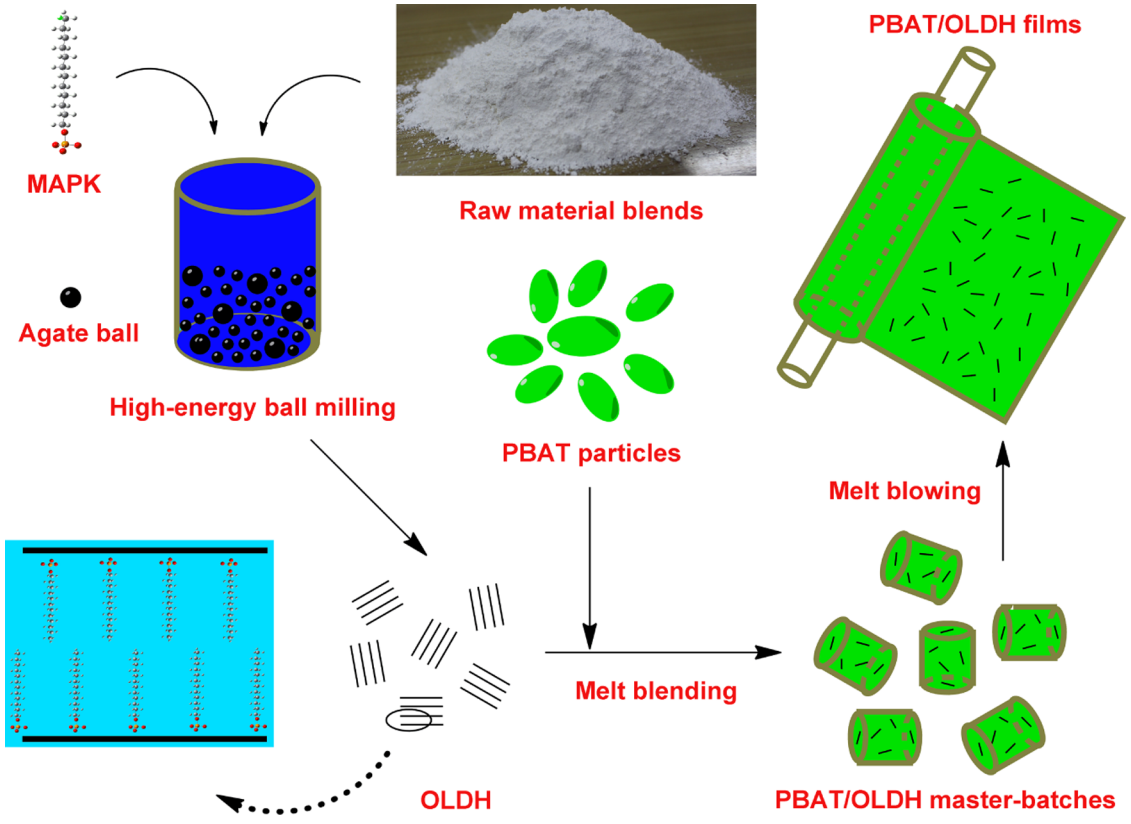

phosphonate anions in the interlayer region. The data collected using a variety of techniques demonstrated that OLDH addition at a loading of ∼1 wt % could significantly enhance the optical and mechanical properties of PBAT, whereas also improving the general processability of the PBAT-based films. The SEM investigations confirmed a very uniform distribution of the OLDH particles throughout the PBAT/OLDH films, with the partial delamination of the OLDH layers during processing thought to be responsible for the enhanced optical (37% reduction in haze) and mechanical performance (41.9% increase in the nominal tensile strain at break in machine direction) compared to pure PBAT films. The OLDH nanoplatelets also enhanced the water vapor barrier properties of the PBAT films by creating a physical obstacle and thus a longer migration path for water molecules. The food packaging measurement revealed that the PBAT/OLDH nanocomposite film containing 1% OLDH showed a better packaging effect than pure PBAT film and commercial polyethylene packing materials. These results suggest that OLDH addition to create polymer−OLDH nanocomposites is a viable approach for enhancing the properties of biodegradable polymer films for food packaging application.

EXPERIMENTAL SECTION

Materials. Poly(butylene adipate-*co*-terephthalate) (trade name: Biocosafe 2003) with melt flow index 4.2 g (10 min)$^{-1}$ (190 °C, 2.16 kg) was supplied by Xinfu Pharmaceutical Co., Ltd. (Hangzhou, China). $Al(NO_3)_3{\cdot}9H_2O$ (AR, 99%), $Zn(NO_3)_2{\cdot}6H_2O$ (AR, 99%), and NaOH (AR, 99%) were purchased from Aladdin Reagent Co., Ltd. (Shanghai, China). Lauryl alcohol phosphoric acid ester potassium (MAPK) (AR, 97%) was obtained from Lihou Chemical Co., Ltd.

DOI: 10.1021/acsomega.7b02062
ACS Omega 2018, 3, 1187−1196

(Guangzhou, China). All of the reagents were analytical grade and used as received. Deionized water was used in all of the experiments.

Synthesis of ZnAl-MAPK OLDH. The organophilic ZnAl-MAPK OLDH was directly synthesized by solvent-free high-energy ball milling using a QM-3SP2 planetary ball mill. A mixture of MAPK (51.3 g, 0.15 mol) and NaOH (19.2 g, 0.48 mol) was premilled for 30 min, followed by addition of $Zn(NO_3)_2{\cdot}6H_2O$ (53.5 g, 0.18 mol) and $Al(NO_3)_3{\cdot}9H_2O$ (22.5 g, 0.06 mol) and milling for a further 30 min. Four agate pots (inner volume: 500 cm^3) and many agate balls (diameter: 6 mm; quantity: 2000; diameter: 10 mm; quantity: 400) were used in a single milling process. The total volume of reactants and agate balls was approximately three-fourths that of the agate pots. The revolution speed and autorotation rate were fixed at 250 and 500 rpm, respectively. After ball milling, the product slurry was washed three times with deionized water and then dried at 70 °C to obtain white ZnAl-MAPK OLDH powders (yield 180 g). The OLDH powders were ground in a mortar and pestle and then passed through an 800 mesh (0.015 mm) sieve before subsequent use in composite manufacture. The ZnAl-MAPK OLDH powder is simply denoted as OLDH in the text below.

Manufacture of PBAT/OLDH Nanocomposite Films. The PBAT/OLDH nanocomposite films were manufactured by melt blending and blowing process. First, PBAT and OLDH were mixed using a SHR-10A high-speed mixer at a rotary speed of 60 rpm for 10 min, and then the resulting mixture was fed into a SHJ135 co-rotating twin-screw extruder operating at a screw speed of 120 rpm with a temperature difference between the feed and die zones of 120−145 °C. The extruded PBAT/OLDH nanocomposite granulates were subsequently melted and blown into films using a SGXM-1800 single-screw film blowing machine operating at 40 rpm and temperatures of 110, 120, 125, and 130 °C along the four barrel zones. The manufacturing process of the PBAT/OLDH nanocomposite films is summarized in Scheme 1. The mass ratios of PBAT and OLDH were 100/0, 99.5/0.5, 99/1, 98/2, and 96/4, respectively, with the corresponding PBAT/OLDH nanocomposite films abbreviated as OLDH-0, OLDH-0.5, OLDH-1, OLDH-2, and OLDH-4 in the text below. For each film, the total mass of PBAT and OLDH was constant (4 kg) and the film thickness controlled at 50 ± 1 μm. The film samples were stored in a desiccator at room temperature before characterization tests.

Characterization. FT-IR spectra were recorded on a Thermo Nicolet 380 spectrometer using the KBr disk method over the range of 4000−400 cm^{-1}. Thirty two consecutive scans collected at a resolution of 4 cm^{-1} were co-added to produce a spectrum. The X-ray diffraction (XRD) patterns were obtained on a Bruker D8 Advance diffractometer, equipped with a Cu Kα source (λ = 1.54056 Å) operating at 40 kV and 40 mA. Data were collected over the 2θ range 1−60°, with a step of 0.02° and a scan speed of 4° min^{-1}. The sample morphologies were examined using an H-800 transmission electron microscope and a JEOL JSM-6380LV scanning electron microscope. The SEM analyses were performed on freeze-fractured PBAT/OLDH films, which were immersed in liquid nitrogen and then fractured. The fractured surfaces were then sputtered coated with gold to improve their conductivity for imaging. The melting and crystallization behavior of the PBAT/OLDH films were investigated using a Netzsch DSC 200PC differential scanning calorimeter under a nitrogen atmosphere (flow rate of 50 mL min^{-1}). The PBAT/OLDH film samples (8−10 mg) were heated from ambient temperature to 200 °C at 10 °C min^{-1} and then held at 200 °C for 3 min to erase the thermal history, after which they were cooled to 0 °C at 10 °C min^{-1} to study the crystallization behavior and finally reheated to 200 °C at 10 °C min^{-1} to study their melting behavior. The optical properties of the PBAT/OLDH films were examined using an INESA WGT-2S light transmittance/haze tester using GB 2410-2008. Optical photographs of the films were taken with a Canon EOS-700d digital camera. The tensile tests on the PBAT/OLDH films were conducted at ambient temperature using a SUNS UTM2502 electronic universal testing machine. The crosshead speed was set at 200 mm min^{-1}. The sample films were cut into dumbbell-shaped pieces according to the GB/T 1040.3-2006 standard. Five specimens of each PBAT/OLDH films were measured and the average reported. The water vapor transmission rate (WVTR) of the PBAT/OLDH films was determined using a PERME W3/030 automatic water vapor transmission tester. The experiments were conducted at a temperature of 23 °C under 57% relative humidity conditions according to the GB 1037-88 standard. Before the measurements, the films were placed in a vacuum drying oven at 60 °C for 12 h to remove the moisture. The films were cut into circles of diameter 0.074 m for the measurements. Three specimens of each PBAT/OLDH film were measured and the average value reported.

■ ASSOCIATED CONTENT

Supporting Information

The Supporting Information is available free of charge on the ACS Publications website at DOI: 10.1021/acsomega.7b02062.

Photograph of the condensation of the water droplet of banana packed by commercial polyethylene packing film; food packaging experiment packed with different films (PDF)

■ AUTHOR INFORMATION

Corresponding Author

*E-mail: jiaxu@sdau.edu.cn.

ORCID

Yuechao Yang: 0000-0003-4045-0252

Jing Xu: 0000-0003-2935-880X

Notes

The authors declare no competing financial interest.

■ ACKNOWLEDGMENTS

This work was supported by the National Key R&D Program of China (Grant No. 2016YFB0302403), the Major Scientific and Technological Innovation Projects (Grant No. 310139), the Project of Shandong Province Education Department (Grant No. ZR2014JL023), the National Natural Science Foundation of China (Grant No. 31572201), and Shandong Youth Education Science Program for College Students (Grant No. 17BSH113). We thank Y.F. for his assistant in the revision of our manuscript.

■ REFERENCES

(1) Morelli, C. L.; Belgacem, M. N.; Branciforti, M. C.; Bretas, R. E.; Crisci, A.; Bras, J. Supramolecular aromatic interactions to enhance biodegradable film properties through incorporation of functionalized cellulose nanocrystals. *Composites, Part A* **2016**, *83*, 80−88.

DOI: 10.1021/acsomega.7b02062
ACS Omega 2018, 3, 1187−1196

(2) Piekarska, K.; Sowinski, P.; Piorkowska, E.; Haque, M. M.-U.; Pracella, M. Structure and properties of hybrid PLA nanocomposites with inorganic nanofillers and cellulose fibers. *Composites, Part A* **2016**, *82*, 34−41.
(3) El Miri, N.; Abdelouahdi, K.; Barakat, A.; Zahouily, M.; Fihri, A.; Solhy, A.; El Achaby, M. Bio-nanocomposite films reinforced with cellulose nanocrystals: Rheology of film-forming solutions, transparency, water vapor barrier and tensile properties of films. *Carbohydr. Polym.* **2015**, *129*, 156−167.
(4) Youssef, A. M.; El-Sayed, S. M.; Salama, H. H.; El-Sayed, H. S.; Dufresne, A. Evaluation of bionanocomposites as packaging material on properties of soft white cheese during storage period. *Carbohydr. Polym.* **2015**, *132*, 274−285.
(5) Dhar, P.; Gaur, S. S.; Soundararajan, N.; Gupta, A.; Bhasney, S. M.; Kumar, A.; Katiyar, V.; et al. Reactive extrusion of polylactic acid/cellulose nanocrystal films for food packaging applications: Influence of filler type on thermo-mechanical, rheological and barrier properties. *Ind. Eng. Chem. Res.* **2017**, *56*, 4718−4735.
(6) Çoban, O.; Bora, M. Ö.; Kutluk, T.; Özkoç, G. Mechanical and thermal properties of volcanic particle filled PLA/PBAT composites. *Polym. Compos.* **2017**, DOI: 10.1002/pc.24393.
(7) Li, R. Y.; Wu, L. B.; Li, B. G. Poly(l-lactide) materials with balanced mechanical properties prepared by blending with PEG-mb-PPA multiblock copolymers. *Ind. Eng. Chem. Res.* **2017**, *56*, 2773−2782.
(8) Zheng, F.; Mi, Q. H.; Zhang, K.; Xu, J. Synthesis and characterization of poly(propylene carbonate)/modified sepiolite nanocomposites. *Polym. Compos.* **2016**, *37*, 21−27.
(9) Zhou, L. Y.; Zhao, G. Y.; Jiang, W. Effects of catalytic transesterification and composition on the toughness of poly(lactic acid)/poly(propylene carbonate) blends. *Ind. Eng. Chem. Res.* **2016**, *55*, 5565−5573.
(10) Li, S.; Deng, L.; Xu, C.; Wu, Q. H.; Wang, Z. G. Making a supertough flame-retardant polylactide composite through reactive blending with ethylene-acrylic ester-glycidyl methacrylate terpolymer and addition of aluminum hypophosphite. *ACS Omega* **2017**, *2*, 1886−1895.
(11) Wu, N.; Zhang, H. Mechanical properties and phase morphology of super-tough PLA/PBAT/EMA-GMA multicomponent blends. *Mater. Lett.* **2017**, *192*, 17−20.
(12) Nofar, M.; Heuzey, M. C.; Carreau, P. J.; Kamal, M. R. Effects of nanoclay and its localization on the morphology stabilization of PLA/PBAT blends under shear flow. *Polymer* **2016**, *98*, 353−364.
(13) Moustafa, H.; Galliard, H.; Vidal, L.; Dufresne, A. Facile modification of organoclay and its effect on the compatibility and properties of novel biodegradable PBE/PBAT nanocomposites. *Eur. Polym. J.* **2017**, *87*, 188−199.
(14) Lin, S.; Guo, W. N.; Chen, C. Y.; Ma, J.; Wang, B. B. Mechanical properties and morphology of biodegradable poly (lactic acid)/poly (butylene adipate-co-terephthalate) blends compatibilized by transesterification. *Mater. Des.* **2012**, *36*, 604−608.
(15) Fukushima, K.; Wu, M.-H.; Bocchini, S.; Rasyida, A.; Yang, M.-C. PBAT based nanocomposites for medical and industrial applications. *Mater. Sci. Eng., C* **2012**, *32*, 1331−1351.
(16) Raquez, J. M.; Nabar, Y.; Narayan, R.; Dubois, P. Novel high-performance talc/poly [(butylene adipate)-co-terephthalate] hybrid materials. *Macromol. Mater. Eng.* **2008**, *293*, 310−320.
(17) Chieng, B.; Ibrahim, N.; Wan Yunus, W. Effect of organo-modified montmorillonite on poly (butylene succinate)/poly (butylene adipate-co-terephthalate) nanocomposites. *eXPRESS Polym. Lett.* **2010**, *4*, 404−414.
(18) Jo, C. I.; Ko, J. U.; Yin, Z. X.; Kim, Y. J.; Kim, Y. S. Solvent-free and highly transparent SiO_2 nanoparticle-polymer composite with an enhanced moisture barrier property. *Ind. Eng. Chem. Res.* **2016**, *55*, 9433−9439.
(19) Zhang, M.; Wei, T.; Zhang, A. M.; Li, S. L.; Shen, F. C.; Dong, L. Z.; Li, D. S.; Lan, Y. Q. Polyoxomolybdate-polypyrrole/reduced graphene oxide nanocomposite as high-capacity electrodes for lithium storage. *ACS Omega* **2017**, *2*, 5684−5690.
(20) Chen, J.-H.; Yang, M.-C. Preparation and characterization of nanocomposite of maleated poly (butylene adipate-co-terephthalate) with organoclay. *Mater. Sci. Eng., C* **2015**, *46*, 301−308.
(21) Livi, S.; Sar, G.; Bugatti, V.; Espuche, E.; Duchet-Rumeau, J. Synthesis and physical properties of new layered silicates based on ionic liquids: improvement of thermal stability, mechanical behaviour and water permeability of PBAT nanocomposites. *RSC Adv.* **2014**, *4*, 26452−26461.
(22) Xie, W.; Gao, Z. M.; Pan, W.-P.; Hunter, D.; Singh, A.; Vaia, R. Thermal degradation chemistry of alkyl quaternary ammonium montmorillonite. *Chem. Mater.* **2001**, *13*, 2979−2990.
(23) Zhang, J.; Hu, H.; Li, Z.; Lou, X. W. Double-shelled nanocages with cobalt hydroxide inner shell and layered double hydroxides outer shell as high-efficiency polysulfide mediator for lithium-sulfur batteries. *Angew. Chem., Int. Ed.* **2016**, *55*, 3982−3986.
(24) Zhou, C.-H. Emerging trends and challenges in synthetic clay-based materials and layered double hydroxides. *Appl. Clay Sci.* **2010**, *48*, 1−4.
(25) Hennous, M.; Derriche, Z.; Privas, E.; Navard, P.; Verney, V.; Leroux, F. Lignosulfonate interleaved layered double hydroxide: A novel green organoclay for bio-related polymer. *Appl. Clay Sci.* **2013**, *71*, 42−48.
(26) Mohapatra, L.; Parida, K. A review on the recent progress, challenges and perspective of layered double hydroxides as promising photocatalysts. *J. Mater. Chem. A* **2016**, *4*, 10744−10766.
(27) Long, X.; Wang, Z. L.; Xiao, S.; An, Y. M.; Yang, S. H. Transition metal based layered double hydroxides tailored for energy conversion and storage. *Mater. Today* **2016**, *19*, 213−226.
(28) Wang, L. L.; Li, B.; Zhang, X. C.; Chen, C. X.; Zhang, F. Effect of intercalated anions on the performance of Ni-Al LDH nanofiller of ethylene vinyl acetate composites. *Appl. Clay Sci.* **2012**, *56*, 110−119.
(29) Ciou, C.-Y.; Li, S.-Y.; Wu, T.-M. Morphology and degradation behavior of poly(3-hydroxybutyrate-co-3-hydroxyvalerate)/layered double hydroxides composites. *Eur. Polym. J.* **2014**, *59*, 136−143.
(30) Liu, L.; Yu, T.; Wang, G.; Wang, P.; Wei, Z.; Qi, M. Ring-opening polymerization approach to ε-caprolactone grafting onto modified LDH biodegradable nanocomposites. *J. Controlled Release* **2013**, *172*, No. e132.
(31) Chen, Y. A.; Tsai, G. S.; Chen, E. C.; Wu, T. M. Thermal degradation behaviors and biodegradability of novel nanocomposites based on various poly[(butylene succinate)-co-adipate] and modified layered double hydroxides. *J. Taiwan Inst. Chem. Eng.* **2017**, *77*, 263−270.
(32) Zhang, F. R.; Du, N.; Song, S.; Liu, J. Q.; Hou, W. G. Mechano-hydrothermal synthesis of Mg_2Al-NO_3 layered double hydroxides. *J. Solid State Chem.* **2013**, *206*, 45−50.
(33) Iwasaki, T.; Yoshii, H.; Nakamura, H.; Watano, S. Simple and rapid synthesis of Ni−Fe layered double hydroxide by a new mechanochemical method. *Appl. Clay Sci.* **2012**, *58*, 120−124.
(34) Schrijvers, D. L.; Leroux, F.; Verney, V.; Patel, M. K. Ex-ante life cycle assessment of polymer nanocomposites using organo-modified layered double hydroxides for potential application in agricultural films. *Green Chem.* **2014**, *16*, 4969−4984.
(35) Al-Itry, R.; Lamnawar, K.; Maazouz, A. Reactive extrusion of PLA, PBAT with a multi-functional epoxide: physico-chemical and rheological properties. *Eur. Polym. J.* **2014**, *58*, 90−102.
(36) Chen, W.; Qu, B. J. Structural characteristics and thermal properties of PE-g-MA/MgAl-LDH exfoliation nanocomposites synthesized by solution intercalation. *Chem. Mater.* **2003**, *15*, 3208−3213.
(37) Xie, J.; Yang, Y.; Gao, B.; Wan, Y.; Li, Y. C.; Xu, J.; Zhao, Q. Biomimetic Superhydrophobic Biobased Polyurethane-Coated Fertilizer with Atmosphere "Outerwear". *ACS Appl. Mater. Interfaces* **2017**, *9*, 15868−15879.
(38) Ibrahim, N. A.; Rahim, N. M.; Yunus, W. Z. W.; Sharif, J. A study of poly vinyl chloride/poly (butylene adipate-co-terephthalate) blends. *J. Polym. Res.* **2011**, *18*, 891−896.
(39) Gao, Y.; Wu, J.; Zhang, Z.; Jin, R.; Zhang, X.; Yan, X.; Umar, A.; Guo, Z.; Wang, Q. Synthesis of polypropylene/Mg_3Al-X (X = CO_3^{2-},

DOI: 10.1021/acsomega.7b02062
ACS Omega 2018, 3, 1187−1196

NO_3^-, Cl^-, SO_4^{2-}) LDH nanocomposites using a solvent mixing method: thermal and melt rheological properties. *J. Mater. Chem. A* **2013**, *1*, 9928−9934.
(40) Xie, J. Z.; Zhang, K.; Wu, J. F.; Ren, G. F.; Chen, H. Y.; Xu, J. Bio-nanocomposite films reinforced with organo-modified layered double hydroxides: preparation, morphology and properties. *Appl. Clay Sci.* **2016**, *126*, 72−80.
(41) Mathieu, L. M.; Mueller, T. L.; Bourban, P. E.; Pioletti, D. P.; Müller, R.; Månson, J. A. Architecture and properties of anisotropic polymer composite scaffolds for bone tissue engineering. *Biomaterials* **2006**, *27*, 905−916.
(42) Gopakumar, T. G.; Lee, J. A.; Kontopoulou, M.; Parent, J. S. Influence of clay exfoliation on the physical properties of montmorillonite/polyethylene composites. *Polymer* **2002**, *43*, 5483−5491.
(43) Mohanty, S.; Nayak, S. K. Biodegradable nanocomposites of poly (butylene adipate-co-terephthalate) (PBAT) with organically modified nanoclays. *Int. J. Plast. Technol.* **2010**, *14*, 192−212.
(44) Xie, J. Z.; Zhang, K.; Zhao, Q. H.; Wang, Q. G.; Xu, J. Large-scale fabrication of linear low density polyethylene/layered double hydroxides composite films with enhanced heat retention, thermal, mechanical, optical and water vapor barrier properties. *J. Solid State Chem.* **2016**, *243*, 62−69.
(45) Inoue, Y.; Yoshie, N. Structure and physical properties of bacterially synthesized polyesters. *Prog. Polym. Sci.* **1992**, *17*, 571−610.
(46) Żenkiewicz, M.; Richert, J. Permeability of polylactide nanocomposite films for water vapour, oxygen and carbon dioxide. *Polym. Test.* **2008**, *27*, 835−840.
(47) Tas, C. E.; Hendessi, S.; Baysal, M.; Unal, S.; Cebeci, F. C.; Menceloglu, Y. Z.; Unal, H. Halloysite nanotubes/polyethylene nanocomposites for active food packaging materials with ethylene scavenging and gas barrier properties. *Food Bioprocess Technol.* **2017**, *10*, 789−798.

DOI: 10.1021/acsomega.7b02062
ACS Omega 2018, 3, 1187−1196